Article:

Milletari, Mirco and Ferreira, Aires (2016) Crossover to the Anomalous Quantum Regime in the Extrinsic Spin Hall Effect of Graphene. Physical Review B. 201402. ISSN: 2469-9969

https://doi.org/10.1103/PhysRevB.94.201402

PHYSICAL REVIEW B **94**, 201402(R) (2016)

Crossover to the anomalous quantum regime in the extrinsic spin Hall effect of graphene

Mirco Milletarì*
Centre for Advanced 2D Materials and Department of Physics, National University of Singapore, Singapore 117551

Aires Ferreira†
Department of Physics, University of York, York YO10 5DD, United Kingdom

(Received 12 April 2016; published 7 November 2016)

Recent reports of spin-orbit coupling enhancement in chemically modified graphene have opened doors to studies of the spin Hall effect with massless chiral fermions. Here, we theoretically investigate the interaction and impurity density dependence of the extrinsic spin Hall effect in spin-orbit coupled graphene. We present a nonperturbative quantum diagrammatic calculation of the spin Hall response function in the strong-coupling regime that incorporates skew scattering and *anomalous* impurity density-independent contributions on equal footing. The spin Hall conductivity dependence on Fermi energy and electron-impurity interaction strength reveals the existence of experimentally accessible regions where anomalous quantum processes dominate. Our findings suggest that spin-orbit-coupled graphene is an ideal model system for probing the competition between semiclassical and *bona fide* quantum scattering mechanisms underlying the spin Hall effect.

DOI: 10.1103/PhysRevB.94.201402

Spintronics aims to explore charge, spin, and orbital degrees of freedom of electrons to realize novel approaches to advanced storage and logic computing [1]. Graphene—a one-atom-thick layer of carbon atoms with unique electronic properties [2]—holds promising applications in spintronics [3]. The weak spin-orbit coupling [4,5] and high mobilities of sp_2-hybridized carbon result in large spin-diffusion lengths (e.g., 1–20-μm in exfoliated samples [6,7]), making graphenic systems attractive as spin channels of high performance [6–8].

Recent progress in engineering of enhanced spin-orbit coupling (SOC) in graphene through addition of impurities [9,10] and via coupling to suitable substrates [11–14] opens up intriguing possibilities. The presence of spin-orbit interactions is predicted to profoundly alter the standard pictures of spin relaxation [15,16] and weak localization [17]. Furthermore, a sizable SOC enables spin-dependent transport phenomena absent in pristine samples [18–22], most noticeably the spin Hall effect (SHE), whereby charge currents driven by electric fields are converted to transverse spin currents [23–25]. This phenomenon was first observed by optical means in semiconductors in 2004 [26,27], and its reciprocal—the inverse SHE—just shortly after demonstrated by direct electrical measurements in metals [28,29]. According to theory, a modest SOC in the range of 10 meV in graphene enables robust and gate-tunable SHE [18]. Recent reports on SHE exploring Hanle precession in adatom-decorated graphene [9,10] and graphene-WS_2 heterostructures [12,13], and spin pumping in graphene/YIG devices [14], confirm theoretical predictions, and pave the way for *all electric* spintronics in graphene.

Generally, two types of SHE can occur in a spin-orbit-coupled graphene system. When charge carriers experience a *global* SOC—endowed by proximity effect—a SHE is induced by the Berry curvature of Bloch bands (the so-called "intrinsic mechanism"), with scattering-dependent corrections due to disorder [30]. Conversely, if the SOC enhancement is confined to random "hot spots"—e.g., as mediated by impurities—two basic mechanisms can compete to establish a SHE, *viz.*, the left/right asymmetric (skew) scattering for spin-up and spin-down electrons [18,19], and the quantum side-jump (QSJ) effect. The latter can be viewed as a coordinate shift of wave packets upon scattering in the presence of SOC. The side jump is transverse to the external electric field and has opposite signs for spin-up/down electrons, which results in a net contribution to the spin Hall conductivity [30–34].

Owing to the sharpness of resonant scattering characteristic of massless fermions in two dimensions [35–38], the extrinsic SHE induced by skew scattering from SOC-active impurities in graphene is predicted to be extremely robust, capable of yielding giant spin Hall angles of the order of 0.1 [18,19,39]. For a very low concentration of impurities, quantum contributions to the spin Hall (SH) conductivity are negligible, and the semiclassical skew scattering fully determines the steady state of SHE [18]. However, much less is known about the role of quantum processes in the dilute regime of much interest in extrinsic graphene (≈ 0.01–0.1% atomic ratio [9,10,40]), especially in the strong scattering limit, where quantum contributions to the SH response functions are hard to assess [41].

In this Rapid Communication, we present a microscopic theory of the extrinsic SHE in graphene based on a nonperturbative quantum diagrammatic calculation able to capture the strong scattering regime self-consistently. We find that skew scattering, QSJ, and multiple impurity scattering processes need to be considered *on equal footing* for an accurate description of the extrinsic SHE. Quite remarkably, a crossover towards an "anomalous phase"—where quantum processes overcome skew scattering—is shown to occur in experimentally accessible parameter regions. Our self-consistent approach goes beyond previous theories [18,25,30,31,34], providing a unified description of skew scattering and side-jump mechanisms.

Model system. The low-energy physics of spin-orbit-coupled graphene is described by a Dirac Hamiltonian in two spatial dimensions with a random impurity potential.

*milletari@gmail.com
†aires.ferreira@york.ac.uk

For simplicity, the typical size of SOC-active impurities is assumed much larger than the lattice spacing, hence suppressing intervalley scattering [18,19]. We work with the SO(5) representation of the spin algebra [42,43] in terms of $4 \times 4 = 1 + 5 + 10$ matrices, i.e., one identity, γ^0, five γ^a matrices, taken as $\gamma^1 = \sigma_1 \otimes s_0$, $\gamma^2 = \sigma_2 \otimes s_0$, $\gamma^3 = \sigma_3 \otimes s_3$, $\gamma^4 = \sigma_3 \otimes s_2$, and $\gamma^5 = \sigma_3 \otimes s_1$, and ten adjoint matrices $\gamma^{ab} = i/2\,[\gamma^a,\gamma^b]$. Here $\boldsymbol{\sigma}$ and $\boldsymbol{s}$ are Pauli matrices defined in the sublattice and spin space, respectively. The Hamiltonian density reads

$$\mathscr{H} = \psi^\dagger(\mathbf{x})\{-i\,v\,\gamma^a\partial_a - \gamma_0\,\epsilon + V(\mathbf{x})\}\psi(\mathbf{x}), \tag{1}$$

where v is the Fermi velocity of charge carriers, ϵ is the Fermi energy, and $V(\mathbf{x})$ denotes the disorder potential. Hereafter, we set $\hbar \equiv 1 \equiv e$, unless stated otherwise. The impurities are modeled as short-range potentials, $V(\mathbf{x}) = \sum_{i=1}^N M\,R^2\delta(\mathbf{x} - \mathbf{x}_i)$, where M is a 4×4 matrix encoding the spin and sublattice structure of the impurity, and R is a length scale mimicking a potential range [38]. We posit our analysis on impurities leading to a SOC of the "intrinsic type" [4,5] and allow for an extra (scalar) electrostatic term in the impurity matrix:

$$M = \alpha_0\,\gamma_0 + \alpha_3\,\gamma_3, \tag{2}$$

with α_0 (α_3) denoting the magnitude of the scalar (SOC) component of the disordered potential. Note that γ_3 conserves the out-of-plane spin component, in addition to being an invariant of the C_{6v} point group, and thus is the simplest form of SOC in graphene; physical realizations include physisorbed atoms in the hollow position, and top-position adatoms randomly distributed over sublattices [19,44].

Methodology. Being interested in the effect of asymmetric and strong scattering, the standard *Gaussian white noise* approximation is not applicable. Instead, we employ the T-matrix approach valid for a low density of impurities with otherwise arbitrarily strong scattering potential. The T matrix is the result of an infinite order resummation of potential scattering diagrams containing only one impurity density insertion $n = N/\Omega$ (here Ω is the sample area) in the noncrossing approximation [41]. The self-energy reads $\Sigma(\epsilon) = n\,\langle T(\epsilon)\rangle_{\text{dis}}$, where $\langle \ldots \rangle_{\text{dis}}$ denotes configurational average. We find, after ressumation, $\langle T(\epsilon)\rangle_{\text{dis}} = \frac{1}{2}(T_+ + T_-)\gamma_0 + \frac{1}{2}(T_+ - T_-)\gamma_3 \equiv T$, with

$$T_\pm = \frac{R^2\,(\alpha_0 \pm \alpha_3)}{1 - R^2\,(\alpha_0 \pm \alpha_3)\,g_0(\epsilon)} \equiv \epsilon_\pm \mp i\,\eta_\pm. \tag{3}$$

In the above, $g_0(\epsilon) = -\epsilon/2\pi v^2 \ln(\Lambda/|\epsilon|) \mp i\,|\epsilon|/4v^2$ is the momentum integrated bare propagator in retarded (advanced) sectors, and Λ is a high-energy cutoff [38]. To simplify notation, hereafter $\epsilon > 0$ is assumed. It is convenient to decompose the self-energy in real and imaginary parts as $\mathrm{Re}\,\Sigma = n(\delta\epsilon\,\gamma_0 + m\,\gamma_3)$ and $-\mathrm{Im}\,\Sigma = n(\eta\,\gamma_0 + \bar{\eta}\,\gamma_3)$, where $\delta\epsilon = (\epsilon_+ + \epsilon_-)/2$, $m = (\epsilon_+ - \epsilon_-)/2$, $\eta = (\eta_+ + \eta_-)/2$, and $\bar{\eta} = (\eta_+ - \eta_-)/2$. Here, $n\,\delta\epsilon$ is a chemical potential shift that can be reabsorbed in ϵ, while $n\,m$ is a (small) disorder-induced SOC gap. This result shows that $\hat{\Sigma}$ endows quasiparticles with two different lifetimes; we have defined $n\,\eta$ and $n\,\bar{\eta}$ as the respective energy and spin gap broadenings. The disorder averaged propagator reads

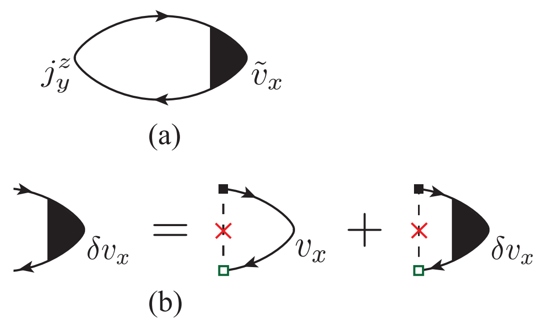

FIG. 1. Kubo-Streda diagrams. (a) Response bubble for the SH conductivity with dressed charge vertex $\tilde{v}_x = v_x + \delta v_x$. (b) Bethe-Salpeter equation for the vertex correction δv_x.

$$\mathcal{G}^{R/A}_{\mathbf{k}}(\epsilon) = \frac{(\epsilon \pm i\,n\,\eta)\gamma_0 + n\,(m \mp i\,\bar{\eta})\gamma_3 + v\,\gamma^j k_j}{(\epsilon \pm i\,n\,\eta)^2 - n^2(m \mp i\,\bar{\eta})^2 - v^2\,k^2}. \tag{4}$$

It is interesting to note that the above propagator has a structure similar to that found in minimal models of the anomalous Hall effect (AHE) based on the massive Dirac equation in $d = 2 + 1$ [45,46] (note, however, the physically distinct origins of the respective γ_3 "mass" terms). Next, we evaluate the SH conductivity using the Kubo-Streda formula, represented diagrammatically in Fig. 1. In our model, the spin and charge vertex are given, respectively, by $j_y^z = v/2\,\gamma_{13}$ and $v_x = v\,\gamma_1$.

Bubble approximation; unitary vs Gaussian limits. It is instructive to first consider the limiting cases of infinitely strong (unitary) and weak (Gaussian) scatterers. Neglecting the vertex corrections for the moment, we obtain to leading order in the impurity density, and including a valley degeneracy factor of 2:

$$\sigma^0_{\text{SH}} = 2\int \frac{d^2\mathbf{k}}{(2\pi)^2}\,\mathrm{Tr}\big[\,j_y^z\,\mathcal{G}^R_{\mathbf{k}}(\epsilon)\,v_x\,\mathcal{G}^A_{\mathbf{k}}(\epsilon)\,\big] \simeq \frac{\bar{\eta}}{\eta}. \tag{5}$$

The bubble SH conductivity is a ratio of two broadening scales and hence is independent on the impurity density; the underlying SH mechanism is the QSJ [32]. In the *unitary* limit, $|\mathrm{Re}\,g_0\,R^2(\alpha_0 \pm \alpha_3)| \gg 1$, $\eta_\pm \approx \pi^2 v^2/\epsilon \ln(\Lambda/\epsilon)$, and hence the SH conductivity is identically zero. On the other hand, in the *Gaussian* limit, $|\mathrm{Re}\,g_0\,R^2(\alpha_0 \pm \alpha_3)| \ll 1$, $\eta_\pm \simeq R^4(\alpha_0 \pm \alpha_3)^2\epsilon/(4v^2)$, and one obtains a nonzero result, $\sigma^0_{\text{SH}} = 2\,\alpha_0\,\alpha_3/(\alpha_0^2 + \alpha_3^2)$. The Gaussian approximation then gives an energy independent contribution, while dependence on the Fermi energy only appears at order n and it is therefore subleading in the dilute regime. However, a careful analysis shows that this result is an artifact of the Gaussian approximation. In order to obtain the correct dependence on the Fermi energy, a calculation based on the full T-matrix approach is required.

Full calculation. The T matrix enters the problem in the propagators (via self-energy) and in the response bubble itself (four-point function). The former has already been evaluated below Eq. (3); we now tackle the four-point function. Figure 2 shows the dressed ladder diagram and its skeleton expansion. In order to describe the strong scattering regime, one needs to change the Feynman's rules for disorder potential

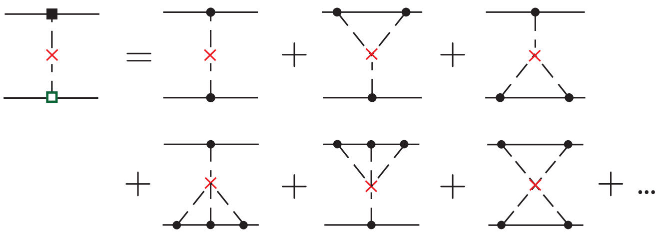

FIG. 2. T Matrix ladder. Skeleton expansion of the ladder diagram in terms of an infinite series of two particle, noncrossing diagrams. On the left side, a full (open) square interaction vertex denotes a T (T^*) matrix insertion, while on the right the T matrix is expanded in its bare components (M insertions). The red $\times$ represents an impurity density insertion.

insertions from the standard bare interaction (dot) to the T-matrix-dressed one (squares). This procedure generates *all diagrams* with one impurity density insertion (one $\times$), thus providing an accurate nonperturbative result. The treatment of four-point electron-hole propagators at the T-matrix level has been employed in Ref. [47] in the context of resonant scattering in anisotropic superconductors. Although previously neglected in studies of anomalous and SH effects, the additional (four-point) diagrams are essential to describe the strong scattering regime relevant for SHE in spin-orbit-coupled graphene. In the skeleton expansion of Fig. 2, one recognizes the first term as the bare ladder diagram, providing the first correction to the empty bubble, Eq. (5). The next two diagrams in the figure ("Y diagrams") contain three M impurity insertions, and hence encode skew scattering (SS) at the lowest order [30,32,45,48]. The remaining diagrams build up the complete four-point skeleton series describing QSJ and SS processes at all orders in the impurity potential.

The charge vertex is schematically shown in Fig. 1, together with the conductivity diagram. We first evaluate the single-impurity vertex correction $\bar{v}_x$. Using the T-matrix ladder diagram shown in Fig. 2, we find

$$\begin{aligned}\bar{v}_x &= n \int \frac{d^2\mathbf{k}}{(2\pi)^2}\, T\, \mathcal{G}^R_{\mathbf{k}}\, v_x\, \mathcal{G}^A_{\mathbf{k}}\, T^* = v\,(a\,\gamma_1 + b\,\gamma_{13}),\\ a &\simeq \epsilon\, \frac{\eta_+\,\eta_- + \epsilon_+\,\epsilon_-}{4v^2(\eta_+ + \eta_-)} - n\, f_a(\eta_+,\eta_-,\epsilon_+,\epsilon_-),\\ b &\simeq \epsilon\, \frac{\eta_+\,\epsilon_- - \eta_-\,\epsilon_+}{4v^2(\eta_+ + \eta_-)} + n\, f_b(\eta_+,\eta_-,\epsilon_+,\epsilon_-),\end{aligned} \tag{6}$$

where f_a and f_b are complicated functions of $\eta_\pm,\epsilon_\pm$; explicit expressions are given in the Supplemental Material (SM) [49]. Note that contrary to the Gaussian case, also b contains an n independent contribution. This term is responsible for the semiclassical SS, yielding the standard skew relaxation-time contribution, $\sigma_{\mathrm{SS}} \propto \tau_\perp \propto 1/n$ [18,48]. The only matrix elements contributing to the vertex renormalization are those proportional to γ_1 and γ_{13}. We thus decompose the vertex part in Fig. 1(b) as $\delta v_x = \delta v_x^1\,\gamma_1 + \delta v_x^2\,\gamma_{13}$. Solving the respective Bethe-Salpeter equation, and taking the trace of δv_x together with γ_1 or γ_{13}, we obtain $\tilde{v}_x = (v + \delta v_{10} + n\,\delta v_{11})\,\gamma_1 + (\delta v_{20} + n\,\delta v_{22})\,\gamma_{13}$. For details on the functions δv_{ij} refer to the SM [49]. Substituting the bare vertex in Eq. (5) with the renormalized one, the SH conductivity, in the noncrossing approximation, and to leading order in n reads

$$\begin{aligned}\sigma_{\mathrm{SH}} &= \frac{\epsilon\,\delta v_{20}}{2\,n\,v\,\eta} + \bigg\{\frac{\epsilon\,\delta v_{22} + 2\,(v + \delta v_{10})\,\bar{\eta}}{2\,v\,\eta}\\ &\quad - \delta v_{20}\bigg(\frac{1}{\pi\,v} + \frac{\bar{\eta}\,m}{2\,v\,\eta^2}\bigg)\bigg\}\\ &\equiv \mathcal{S}(\epsilon)/n + \mathcal{Q}_{\mathrm{nc}}(\epsilon),\end{aligned} \tag{7}$$

the main result of the Rapid Communication. The semiclassical $\mathcal{O}(n^{-1})$ contribution is due to SS, whereas the term in brackets, $\mathcal{Q}_{\mathrm{nc}}(\epsilon)$, here referred to as the *anomalous* SH conductivity, has contributions stemming from several mechanisms as described below. In Fig. 3, we plot the SS contribution as a function of the electrostatic potential for typical dilute impurity density and SOC magnitude. There is a parametrically wide region where the SH conductivity attains large Fermi-energy sensitive values. Generally, the SH angle $\gamma = \sigma_{\mathrm{SH}}/\sigma_{xx}$ induced by skew scattering has the following scaling $\gamma \propto n/n^*$, where n^* is the areal density of (SOC inactive) contaminants and we assumed $n \ll n^*$ (in the opposite limit, γ is independent of n). This shows that the SH angle increases linearly with the SOC impurity density in disordered samples where other mechanisms limit the charge mobility. The SS contribution is larger away from neutrality, and tends to zero as the impurity scalar energy scale α_0 is increased, in agreement with the unitary limit result of Eq. (5). The giant SS contribution to the SH conductivity has been demonstrated earlier by means of Boltzmann transport theory [18]. However, to our knowledge, a self-consistent treatment of the spin Hall conductivity, incorporating SS and anomalous processes on equal footing, had not been reported until now.

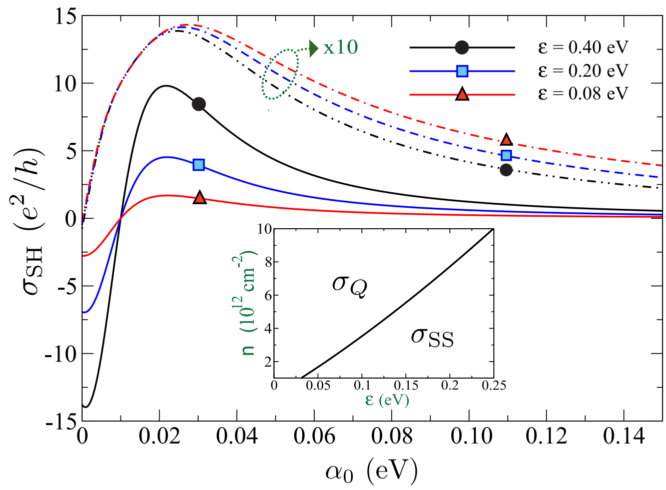

FIG. 3. SH conductivity. The semiclassical SS and anomalous contributions to σ_{SH} are shown for different values of the Fermi energy in solid and dotted lines, respectively. σ_{SS} (σ_Q) increases (decreases) with ϵ, and both conductivities decrease at increasing scalar potential magnitude, in agreement with the unitary limit result. Note that σ_Q has been scaled by a factor of 10. We have used $\alpha_3 = 0.01$ eV, $R = 4$ nm, and $n = 4\times 10^{12}$ cm^{-2}, typical parameters for physisorbed metal nanoparticles [10,18]. The inset shows the regions (ϵ,n) dominated by the semiclassical and anomalous contributions ($\alpha_0 = 0.05$ eV, other parameters as in main figure).

Crossover to the anomalous phase. The anomalous contribution to the SH conductivity is shown in Fig. 3 (dashed lines). It reaches large values of the order of the quantum of conductance and, contrary to what is found for the skew scattering, it increases as the Fermi energy is lowered. Owing to the n^{-1} scaling of the SS contribution, one would naively expect anomalous effects to be negligible in the entire dilute regime. Remarkably, however, a careful inspection of the energy dependence of the spin Hall conductivity discloses parameter regions where anomalous effects are dominant in fairly dilute samples, $|\mathcal{Q}_{\rm nc}(\epsilon)| > |\mathcal{S}(\epsilon)/n|$—see inset to Fig. 3. The rich transport mechanisms at play in the anomalous "phase" are borne out by the distinct contributions appearing inside brackets in Eq. (7). In particular, the vertex part associated to the SS (δv_{20}) also enters the expression for the anomalous term (traditionally associated with pure QSJ events). Interestingly, our nonperturbative calculation shows that diffusion corrections from *reducible* SS diagrams (e.g., diagrams with several "Ys" in Fig. 2) strongly renormalize the anomalous term. Consequently, *even at the level of a single impurity scattering event*, SS and QSJ cannot be treated as separate contributions and a correct evaluation of the anomalous term requires to go beyond the conventional ladder approximation (see Ref. [48] for details).

The characteristic scalings of the semiclassical SS and anomalous contributions together with their sharp variation with Fermi energy provides a smoking gun for an experimental demonstration. In Fig. 4 we present a representative ϵ vs α_0 "phase diagram" of the extrinsic SHE in the intermediate dilute regime, $n \approx 10^{12}$ cm^{-2}, of much experimental relevance. The black line shows the "phase boundary" between a $\mathcal{Q}_{\rm nc}(\epsilon)$- or $\mathcal{S}(\epsilon)/n$-dominated SHE. The narrow region at the bottom of the phase diagram corresponds to the special case with $|\alpha_0| = |\alpha_3|$, for which $\mathcal{S}(\epsilon)/n = 0$ irrespectively of ϵ, cf. Fig. 3. For this particular value, $\mathcal{Q}_{\rm nc}(\epsilon)$ is the only nonzero contribution, hence the particular shape of the phase boundary.

Our results summarized in the inset to Figs. 3 and 4 show that varying the gate voltage (Fermi energy), or alternatively the impurity concentration, enables us to change from a SHE dominated by the semiclassical SS mechanism to a rich quantum transport regime, characterized by correlated SS and QSJ events. Since our calculations are based on a rather conservative model for the impurity resonance, and thermal effects do not destroy the robustness of the extrinsic SHE in graphene [18], the anomalous contributions described

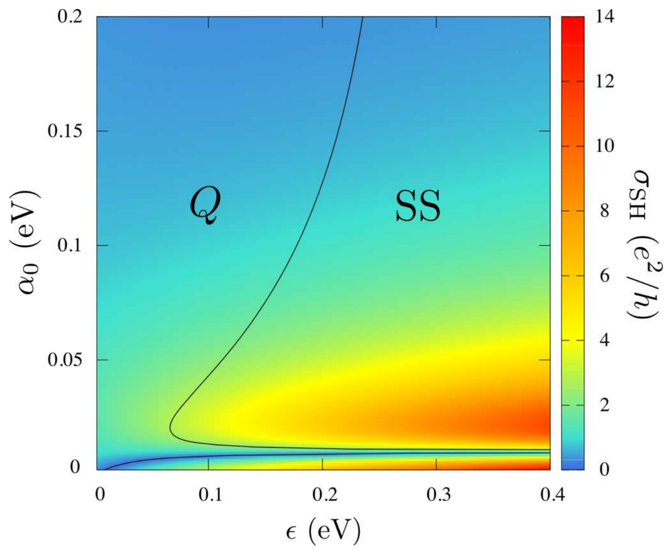

FIG. 4. Phase diagram of the SH conductivity in our model. The diagram shows the parameter regions in which either σ_Q or $\sigma_{\rm SS}$ is dominant. The black line is the phase boundary and the different colors represent the absolute value of $\sigma_{\rm SH}$. We have used $\alpha_3 = 0.01$ eV, $R = 4$ nm, and $n = 4 \times 10^{12}$ cm^{-2}.

here are likely to contribute to nonlocal signals of recent SH experiments [9,10,12–14].

Summary. In this work we unveiled an anomalous quantum regime of the extrinsic spin Hall effect in disordered graphene. Our microscopic theory—based on a powerful nonperturbative treatment of the Kubo-Streda formula—predicts an experimentally accessible crossover from skew scattering- to quantum processes-dominated spin transport, a finding of fundamental importance to the spin Hall and related effects. Our work opens the exciting prospect of probing quantum spin transport phenomena through electrical measurements in graphene and related heterostructures.

Acknowledgments. M.M. thanks R. Raimondi and G. Vignale for stimulating discussions. M.M. acknowledges support from the Singapore National Research Foundation under its fellowship program (NRF Award No. NRF-NRFF2012-01). A.F. gratefully acknowledges the financial support of the Royal Society (U.K.) through a Royal Society University Research Fellowship.

[1] S. A. Wolf, D. D. Awschalom, R. A. Buhrman, J. M. Daughton, S. von Molnár, M. L. Roukes, A. Y. Chtchelkanova, and D. M. Treger, Science **294**, 1488 (2001).

[2] A. H. Castro Neto, F. Guinea, N. M. R. Peres, K. S. Novoselov, and A. K. Geim, Rev. Mod. Phys. **81**, 109 (2009).

[3] W. Han, R. K. Kawakami, M. Gmitra, and J. Fabian, Nat. Nanotechnol. **9**, 794 (2014).

[4] D. Huertas-Hernando, F. Guinea, and A. Brataas, Phys. Rev. B **74**, 155426 (2006).

[5] S. Konschuh, M. Gmitra, and J. Fabian, Phys. Rev. B **82**, 245412 (2010).

[6] C. Jozsa, M. Popinciuc, H. T. Jonkman, and B. J. van Wees, Nature (London) **448**, 571 (2007).

[7] P. J. Zomer, M. H. D. Guimarães, N. Tombros, and B. J. van Wees, Phys. Rev. B **86**, 161416(R) (2012).

[8] W. Han, K. Pi, K. M. McCreary, Y. Li, J. J. I. Wong, A. G. Swartz, and R. K. Kawakami, Phys. Rev. Lett. **105**, 167202 (2010).

[9] J. Balakrishnan, G. K. W. Koon, M. Jaiswal, A. H. C. NeA. H. Castro Netoto, and B. Özyilmaz, Nat. Phys. **9**, 284 (2013).

[10] J. Balakrishnan, G. K. W. Koon, A. Avsar, Y. Ho, J. H. Lee, M. Jaiswal, S.-J. Baeck, J.-H. Ahn, A. Ferreira, M. A. Cazalilla, A. H. Castro Neto, B. Ozyilmaz, Nat. Commun. **5**, 4748 (2014).

[11] D. Marchenko, A. Varykhalov, M. R. Scholz, G. Bihlmayer, E. I. Rashba, A. Rybkin, A. M. Shikin, and O. Rader, Nat. Commun. **3**, 1232 (2012).
[12] A. Avsar, J. Y. Tan, T. Taychatanapat, J. Balakrishnan, G. K. W. Koon, Y. Yeo, J. Lahiri, A. Carvalho, A. S. Rodin, E. C. T. O'Farrell, G. Eda, A. H. Castro Neto, and B. Ozyilmaz, Nat. Commun. **5**, 4875 (2014).
[13] Z. Wang, D.-K. Ki, H. Chen, H. Berger, A. H. MacDonald, and A. F. Morpurgo, Nat. Commun. **6**, 8339 (2015).
[14] J. B. S. Mendes, O. Alves Santos, L. M. Meireles, R. G. Lacerda, L. H. Vilela-Leo, F. L. A. Machado, R. L. Rodríguez-Suárez, A. Azevedo, and S. M. Rezende, Phys. Rev. Lett. **115**, 226601 (2015).
[15] D. V. Fedorov, M. Gradhand, S. Ostanin, I. V. Maznichenko, A. Ernst, J. Fabian, and I. Mertig, Phys. Rev. Lett. **110**, 156602 (2013).
[16] J. Bundesmann, D. Kochan, F. Tkatschenko, J. Fabian, and K. Richter, Phys. Rev. B **92**, 081403(R) (2015).
[17] E. McCann and Vladimir I. Fal'ko, Phys. Rev. Lett. **108**, 166606 (2012).
[18] A. Ferreira, T. G. Rappoport, M. A. Cazalilla, and A. H. Castro Neto, Phys. Rev. Lett. **112**, 066601 (2014).
[19] A. Pachoud, A. Ferreira, B. Özyilmaz, and A. H. Castro Neto, Phys. Rev. B **90**, 035444 (2014).
[20] V. K. Dugaev, E. Y. Sherman, and J. Barnas, Phys. Rev. B **83**, 085306 (2011).
[21] M. M. Asmar and S. E. Ulloa, Phys. Rev. B **87**, 075420 (2013); **91**, 165407 (2015).
[22] A. Dyrdał and J. Barnas, Phys. Rev. B **92**, 165404 (2015).
[23] M. I. D'yakonov and V. I. Perel', ZhETF Pis. Red. **13**, 657 (1971) [JETP Lett. **13**, 467 (1971)].
[24] J. E. Hirsch, Phys. Rev. Lett. **83**, 1834 (1999).
[25] S. Zhang, Phys. Rev. Lett. **85**, 393 (2000).
[26] Y. K. Kato, R. C. Myers, A. C. Gossard, and D. D. Awschalom, Science **306**, 1910 (2004).
[27] J. Wunderlich, B. Kaestner, J. Sinova, and T. Jungwirth, Phys. Rev. Lett. **94**, 047204 (2005).
[28] E. Saitoh, M. Ueda, H. Miyajima, and G. Tatara, Appl. Phys. Lett. **88**, 182509 (2006).
[29] S. O. Valenzuela and M. Tinkham, Nature (London) **442**, 176 (2006).
[30] A. Crepieux and P. Bruno, Phys. Rev. B **64**, 014416 (2001).
[31] P. M. Levy, Phys. Rev. B **38**, 6779 (1988).
[32] N. A. Sinitsyn, J. Phys. Condens. Matter **20**, 023201 (2008).
[33] N. Nagaosa, J. Sinova, S. Onoda, A. H. MacDonald, and N. P. Ong, Rev. Mod. Phys. **82**, 1539 (2010).
[34] P. M. Levy, H. Yang, M. Chshiev, and A. Fert, Phys. Rev. B **88**, 214432 (2013).
[35] T. Stauber, N. M. R. Peres, and F. Guinea, Phys. Rev. B **76**, 205423 (2007).
[36] J. P. Robinson, H. Schomerus, L. Oroszlany, and V. I. Fal'ko, Phys. Rev. Lett. **101**, 196803 (2008).
[37] T. O. Wehling, S. Yuan, A. I. Lichtenstein, A. K. Geim, and M. I. Katsnelson, Phys. Rev. Lett. **105**, 056802 (2010).
[38] A. Ferreira, J. Viana-Gomes, J. Nilsson, E. R. Mucciolo, N. M. R. Peres, and A. H. Castro Neto, Phys. Rev. B **83**, 165402 (2011).
[39] H.-Y. Yang, C. Huang, H. Ochoa, and M. A. Cazalilla, Phys. Rev. B **93**, 085418 (2016).
[40] K. Pi, W. Han, K. M. McCreary, A. G. Swartz, Y. Li, and R. K. Kawakami, Phys. Rev. Lett. **104**, 187201 (2010); X. Hong, S.-H. Cheng, C. Herding, and J. Zhu, Phys. Rev. B **83**, 085410 (2011); A. A. Stabile, A. Ferreira, J. Li, N. M. R. Peres, and J. Zhu, *ibid.* **92**, 121411(R) (2015); B. Yan, Qi Han, Z. Jia, J. Niu, T. Cai, D. Yu, and X. Wu, *ibid.* **93**, 041407(R) (2016).
[41] J. Rammer, *Quantum Transport Theory*, Frontiers in Physics Vol. 99 (Westview Press, Boulder CO, USA, 1998).
[42] A. Zee, *Quantum Field Theory in a Nutshell*, 2nd ed. (Princeton University Press, Princeton, NJ).
[43] S. Murakami, N. Nagaosa, and S. C. Zhang, Phys. Rev. B **69**, 235206 (2004).
[44] M. Gmitra, D. Kochan, and J. Fabian, Phys. Rev. Lett. **110**, 246602 (2013); S. Irmer, T. Frank, S. Putz, M. Gmitra, D. Kochan, and J. Fabian, Phys. Rev. B **91**, 115141 (2015).
[45] N. A. Sinitsyn, A. H. MacDonald, T. Jungwirth, V. K. Dugaev, and J. Sinova, Phys. Rev. B **75**, 045315 (2007).
[46] A. Ado, I. A. Dmitriev, P. M. Ostrovsky, and M. Titov, Europhys. Lett. **111**, 37004 (2015).
[47] P. J. Hirschfeld, P. Wölfle, and D. Einzel, Phys. Rev. B **37**, 83 (1988).
[48] M. Milletarì and A. Ferreira, Phys. Rev. B **94**, 134202 (2016).
[49] See Supplemental Material at http://link.aps.org/supplemental/10.1103/PhysRevB.94.201402 for a detailed derivation of the renormalized vertex.